



ELSEVIER

Available online at [www.sciencedirect.com](http://www.sciencedirect.com)

SCIENCE @ DIRECT®

CONTINENTAL SHELF  
RESEARCH

Continental Shelf Research 25 (2005) 539–555

[www.elsevier.com/locate/csr](http://www.elsevier.com/locate/csr)

# Modification to the atmospheric correction of SeaWiFS ocean colour images over turbid waters

S.J. Lavender<sup>a,b,\*</sup>, M.H. Pinkerton<sup>c</sup>, G.F. Moore<sup>d,b</sup>, J. Aiken<sup>d,b</sup>,  
D. Blondeau-Patissier<sup>d</sup>

<sup>a</sup>*School of Earth, Ocean and Environmental Sciences (SEOES), University of Plymouth, Plymouth Devon, UK*

<sup>b</sup>*Centre for Observation of Air-Sea Interactions and Fluxes (CASIX)*

<sup>c</sup>*National Institute of Water and Atmospheric Research (NIWA), PO Box 14901, Wellington, New Zealand*

<sup>d</sup>*Plymouth Marine Laboratory, Prospect Place, Plymouth PL1 3DH, UK*

Received 23 July 2002; received in revised form 14 September 2004; accepted 1 October 2004

Available online 31 December 2004

## Abstract

The successful exploitation of remotely sensed observations of water colour in the coastal zone requires atmospheric correction methods that can determine water reflectance from top-of-atmosphere radiometric measurements over waters containing significant non-phytoplanktonic particulate material. These so-called Case II waters often have significant water leaving radiance at near infra-red (NIR) wavelengths which invalidates conventional “dark pixel” atmospheric correction procedures, including those using the Siegel-type NIR iterative-correction scheme. A coupled ocean-atmosphere model is described that solves for water-leaving radiance and atmospheric path radiance over Case II turbid waters from measurements by the NASA ocean colour satellite sensor, SeaWiFS. The theoretical basis of this model is described, together with its implementation within the SeaWiFS data processing system, SeaDAS. The resulting products are validated using five test images of European waters, where the modified atmospheric correction leads to significant increases in normalised water leaving-radiances across the whole spectrum and to fewer negative water leaving radiances.

© 2004 Elsevier Ltd. All rights reserved.

*Keywords:* SeaWiFS; Ocean colour; Case 2; Atmospheric correction; Suspended sediment; Geosensing

## 1. Introduction

Satellite remote sensing of ocean colour is the only way at present to measure synoptically wide-area ocean properties such as phytoplankton abundance, the distribution of suspended particulate matter (SPM) and absorption by coloured

\*Corresponding author. School of Earth, Ocean and Environmental Sciences, University of Plymouth, Portland Square, Plymouth PL4 8AA, UK. Tel.: +44 1752 232460; fax: +44 1752 232406.

*E-mail address:* [s.lavender@plymouth.ac.uk](mailto:s.lavender@plymouth.ac.uk)  
(S.J. Lavender).

Nomenclature	
$\phi$	sun-sensor viewing azimuth difference, degrees
$\lambda$	wavelength, nm
$\theta$	sensor viewing zenith angle (the satellite “look angle”), degrees
$\theta_0$	solar zenith angle, degrees
$\rho$	reflectance, dimensionless
$\rho_a$	multiple scattering aerosol reflectance, dimensionless
$\rho'_a$	$= \rho_a + \rho_{ra}$ , dimensionless
$\rho_r$	Rayleigh reflectance, dimensionless
$\rho_{ra}$	reflectance due to Rayleigh-aerosol interaction, dimensionless
$\rho_{rc}$	Rayleigh corrected top of atmosphere reflectance, dimensionless
$\rho_t$	top of atmosphere reflectance, dimensionless
$\rho_w$	water reflectance (above surface), dimensionless
$a$	absorption coefficient, $m^{-1}$
$a^*$	SPM specific absorption coefficient, $m^2 g^{-1}$
$a_w$	absorption coefficient of pure water, $m^{-1}$
$a_{ysbpa}$	absorption coefficient of bleached particles, $m^{-1}$
$b$	scattering coefficient, $m^{-1}$
$b_b$	backscattering coefficient, $m^{-1}$
$b_{bw}$	backscattering coefficient of pure water, $m^{-1}$
$c$	attenuation coefficient, $m^{-1}$
$D$	Earth–Sun distance factor (Gordon et al., 1983), dimensionless
$d$	sequential day of year (1 to 365), dimensionless
$f/q$	upwelling irradiance/radiance ratio, sr
$F_0$	mean extraterrestrial solar irradiance, $\mu W cm^{-2} nm^{-1}$
$K$	diffuse attenuation coefficient, $m^{-1}$
$L$	radiance, $\mu W cm^{-2} sr^{-1} nm^{-1}$
$M$	two-way air mass, dimensionless
$n$	Ångström exponent, dimensionless
$nL_w$	normalised water-leaving radiance, $\mu W cm^{-2} sr^{-1} nm^{-1}$
SPM	suspended particulate matter (concentration), $g m^{-3}$
$t$	diffuse atmospheric transmittance, dimensionless

dissolved organic matter (CDOM). The Sea-viewing Wide Field-of-view Sensor (SeaWiFS), operated by Orbital Sciences Corporation in conjunction with NASA, started operational measurements in September 1997 with the aim of measuring remotely sensed water reflectance across the visible spectrum with an uncertainty of  $\pm 5\%$  (Hooker et al., 1992).

The standard SeaWiFS method for estimating water-leaving reflectance from top-of-atmosphere measurements is the so-called dark pixel (DP) atmospheric correction method (Gordon, 1997; Gordon and Wang, 1994a; Wang, 2000). The original DP method assumed that there was negligible water leaving radiance in the near infra-red part of the spectrum (NIR, 650–900 nm) in order to estimate top-of-atmosphere radiance due to scattering by atmospheric aerosols in the visible bands. An iterative method

(Siegel et al., 2000) was developed to correct for non-negligible water reflectance in the NIR arising from moderate to high phytoplankton abundances (chlorophyll concentrations greater than  $\sim 2 mg m^{-3}$ ). The modified DP method fails in the presence of even modest quantities of SPM ( $> 2 g m^{-3}$ ) because NIR water-leaving radiance is not negligible, and is not related to phytoplankton abundance. This limitation prevents SeaWiFS measuring water leaving radiance over turbid waters and curtails applications in the coastal zone, such as monitoring sediment transport and observing phytoplankton abundance where it occurs with sediment.

A coupled water-atmosphere model has been developed as a modification to the current SeaWiFS atmospheric correction method to estimate ocean colour from SeaWiFS top-of-atmosphere radiometric measurements where the NIR

water reflectance is principally dependent on suspended sediment concentration. The theoretical basis of the model is described, together with its implementation within the SeaWiFS Data Analysis Software (SeaDAS: Fu et al., 1998), version 4.1. Other methods to atmospherically correct remotely sensed satellite ocean colour data over turbid waters have been developed (e.g. Ruddick et al., 2000), but these often rely on an assumption of spatial homogeneity of aerosol type over at least a portion of the image. The algorithm described in this paper does not rely on such an assumption, and instead performs a truly pixel-by-pixel atmospheric correction of the top-of-atmosphere data. The modified version of SeaDAS was used to process SeaWiFS data from five European coastal regions to give a preliminary qualitative validation of the resulting products.

Atlantic Meridional Transect (AMT) cruises have demonstrated that high quality bio-optical data can be routinely provided in near-real time with satellite images (Aiken et al., 2000). In-situ data from the AMT 12 cruise was used for the validation of the Bright Pixel (BP) atmospheric correction over highly scattering waters caused by a coccolithophore bloom event. In this bloom event the NIR water-leaving radiances are not negligible and so a modified atmospheric correction is required.

## 2. Methodology

### 2.1. SeaWiFS dark pixel atmospheric correction

SeaWiFS measures top-of-atmosphere radiance in eight narrow spectral bands spanning the visible and NIR parts of the spectrum. The bands are centred on 412, 443, 490, 510, 555, 670, 765 and 865 nm, and have full-width half-maximum bandwidths of 20 nm ( $\lambda < 700$  nm) and 40 nm ( $\lambda > 700$  nm). We will work in reflectance rather than radiance in this paper, but the two are exactly interchangeable (Eq. (1), Gordon et al., 1988). All symbols and their units are given at the start of this paper.

$$\rho = \frac{\pi L}{F_0 D \cos \theta_0}, \quad (1)$$

where

$$D = \left[ 1 + 0.0167 \cos \frac{2\pi(d-3)}{365} \right]^2. \quad (2)$$

Top-of-atmosphere reflectance measured by SeaWiFS can be partitioned into the bulk reflectance of the water itself, reflectance of the atmosphere due to backscattering by atmospheric molecules (Rayleigh reflectance), reflectance from backscatter by atmospheric aerosols and reflectance from a combination of molecular and aerosol scattering (Eq. (3)). We assume no contamination by sun glint (Hooker et al., 1992) and negligible reflectance from breaking sea-surface waves (Gordon and Wang, 1994b).

$$\rho_t(\lambda) = \rho_r(\lambda) + \rho_a(\lambda) + \rho_{ra}(\lambda) + \rho_w(\lambda)t(\lambda). \quad (3)$$

Only the water reflectance is influenced directly by the water constituents. The atmospheric correction process calculates and subtracts the other components from the top-of-atmosphere signal (Gordon, 1997). As  $\rho_w$  is typically only 5–20% of the top-of-atmosphere signal, both accurate measurement of top-of-atmosphere reflectance and effective atmospheric correction are needed to obtain precise and accurate  $\rho_w$  data. Details of the implementation of the SeaWiFS standard DP atmospheric correction process within SeaDAS can be found at <http://www.seadas.gsfc.nasa.gov>.

The Rayleigh reflectance at all visible and NIR wavelengths depends on the atmospheric molecular composition of the atmosphere, the sun and viewing geometry (Gordon et al., 1988), and, weakly, on sea-surface roughness (Gordon and Wang, 1992). Rayleigh reflectance can hence be computed with good accuracy without use of the remotely sensed radiometric data. Aerosol reflectance cannot be obtained without a priori knowledge in a similar way, because aerosol optical properties can vary substantially over short time- (few days) and space- (few km) scales. Variations in aerosol and in water optical properties on sub-pixel (<1 km) scales are not considered explicitly (Gordon, 1997). Instead, we consider the “average” values of water constituents and aerosol properties appropriate to each pixel.

The SeaWiFS DP atmospheric correction scheme assumes that the water reflectance in SeaWiFS bands 7 and 8 is small, so that the

Rayleigh-corrected top-of-atmosphere reflectance in these bands is, apart from a small correction to account for NIR reflectance by phytoplankton (Siegel et al., 2000), due to aerosol and Rayleigh-aerosol interaction scattering. The aerosol optical model that best fits the measurements of Rayleigh- and Siegel-corrected reflectance in bands 7 and 8 is chosen from a number of candidate models and used to extrapolate the aerosol and Rayleigh-aerosol interaction reflectances from the NIR to the visible bands. Diffuse atmospheric transmittance is calculated based on the same aerosol models (Wang, 1999a) to obtain estimates of  $\rho_w$  in bands 1–6. The DP method fails when there is appreciable water reflectance in bands 7 and 8 due to non-negligible SPM in the water. This failure typically leads to aerosol reflectance being over-estimated, and gives water reflectance values that are too low, and often negative. The errors are typically worse at shorter wavelengths because the aerosol reflectances have been extrapolated over a greater wavelength range, and errors in estimating the aerosol reflectances are hence magnified.

## 2.2. Bright Pixel atmospheric correction modification

The BP atmospheric correction modification to the SeaWiFS atmospheric correction method partitions the NIR Rayleigh-corrected reflectance into aerosol-related reflectance, and turbid water reflectance only. This partition is possible because the spectral shapes of the aerosol and SPM-dominated water reflectances in the NIR are distinct up to an SPM concentration of  $\sim 200 \text{ g m}^{-3}$ . NIR reflectance due to phytoplankton is assumed to be much less than that due to SPM, and is neglected.

Aerosol reflectance in the NIR is assumed to follow the form of Eq. (4) where  $n$  is the Ångström exponent (Gordon and Wang, 1994a).

$$\frac{\rho_a(\lambda_1) + \rho_{ra}(\lambda_1)}{\rho_a(\lambda_2) + \rho_{ra}(\lambda_2)} = \frac{\rho'_a(\lambda_1)}{\rho'_a(\lambda_2)} = \left(\frac{\lambda_1}{\lambda_2}\right)^n, \quad (4)$$

where  $\rho'_a$  is the top-of-atmosphere reflectance due to aerosol multiple scattering and the combination of aerosol and Rayleigh scattering. The Ångström exponent is approximately  $-1.2$  for continental

aerosols, but may vary between about  $+1$  and  $-2$  for mixtures of maritime, continental and urban aerosols. This gives 670:865 ratios of between 0.7 and 1.7, and 765:865 ratios of between about 0.8 and 1.3.

Water reflectance at a given wavelength is a function of the optical properties of seawater, the optically active water constituents and the solar and viewing geometry. The major coloured water constituents are inorganic SPM, phytoplankton (parameterised by chlorophyll-*a* concentration) and coloured dissolved organic matter (CDOM). The optical effects of CDOM and phytoplankton are assumed to be negligible in the NIR for a first approximation. The effects of naturally occurring variations in temperature and salinity on the optical properties of seawater are generally small, and are neglected (Siegel et al., 2000). We hence have Eq. (5).

$$\rho_w(\lambda) = f(\lambda, \text{SPM}, \theta_0, \theta, \phi). \quad (5)$$

Inorganic suspended particulate material is a complex mixture of particles of different types, shapes and sizes, and its optical properties vary widely across Europe and indeed the world. There is a paucity of field-measurements of NIR reflectance in SPM dominated waters because of well-documented difficulties with making accurate radiometric measurements in the NIR using profiling radiometers (e.g. Siegel et al., 2000; Gordon and Ding, 1992). Instrument self-shading and low signal levels become more significant at longer wavelengths, and 700 nm is generally the upper wavelength limit on such measurements. Techniques exist for making radiometric measurements in the NIR using downward-looking spectrometers from above the sea surface, but correcting for skylight reflected from the sea-surface remains inexact (Hooker et al., 2002). Instead, this study used laboratory measurements of water reflectance in the NIR for different concentrations of sediment collected from a number of UK coastal sites representing diverse sediment mineralogies (Bale et al., 1994).

A nadir viewing spectroradiometer was used to measure above-surface water reflectance from a 2 m-deep tank, illuminated by a 1 kW quartz-halogen lamp at  $45^\circ$ . Various concentrations of

SPM were added to seawater in the tank and vigorously stirred before measurement. The sediment samples were used in their entirety, and also size-fractionated into three parts using a settling column: the coarse fraction settled 1 m in 10 min; the medium fraction took between 10 min and 3 h to settle 1 m; the fine fraction had not settled after 3 h.

Fig. 1 shows that there are good relationships between total SPM concentration and NIR reflectance for any given sediment type, but no consistency in this relationship between different sediment types. The higher reflectance of the finer fractions relative to the coarser fractions is consistent with increasing backscatter by particles closer in size to the wavelength of the light. The relationship between the concentration of the fine sediment fraction and NIR reflectance was relatively consistent between different sites. In addition, the ratio of reflectance at two NIR wavelengths showed a well-behaved relationship, irrespective of sediment type (Fig. 2). The ratio  $\rho_w(670)/\rho_w(865)$  was between 1.2 and 4.1, and the ratio  $\rho_w(765)/\rho_w(865)$  was between about 1.2 and 1.9, for  $0.1 < \text{SPM} < 400 \text{ g m}^{-3}$ . The ratios were smaller at higher SPM concentrations. Fig. 2 also shows the ratio of aerosol reflectance at two different NIR bands for Ångström exponents between  $-1$  and  $+2$ . Fig. 2 shows that it is only possible to distinguish SPM reflectance from aerosol reflectance at nominal SPM concentrations lower than  $\sim 200 \text{ g m}^{-3}$ . At higher concentrations, the NIR signatures of the aerosol and SPM converge and cannot be separated.

An empirical model of sediment NIR reflectance was fitted to the tank measurements using a sediment concentration parameter, SPM. The agreement between the model SPM parameter and actual, total SPM concentration is irrelevant to the aim of partitioning remotely sensed reflectance between the water component and the sediment component. Instead, the model must accurately reproduce variations in the relative reflectances of the water at the NIR wavelengths 670, 765 and 865 nm. We have chosen to fit the model to the NIR reflectance of the fine fraction as it is reasonable to assume that it is the fine SPM fraction in the shallow near-surface layer which

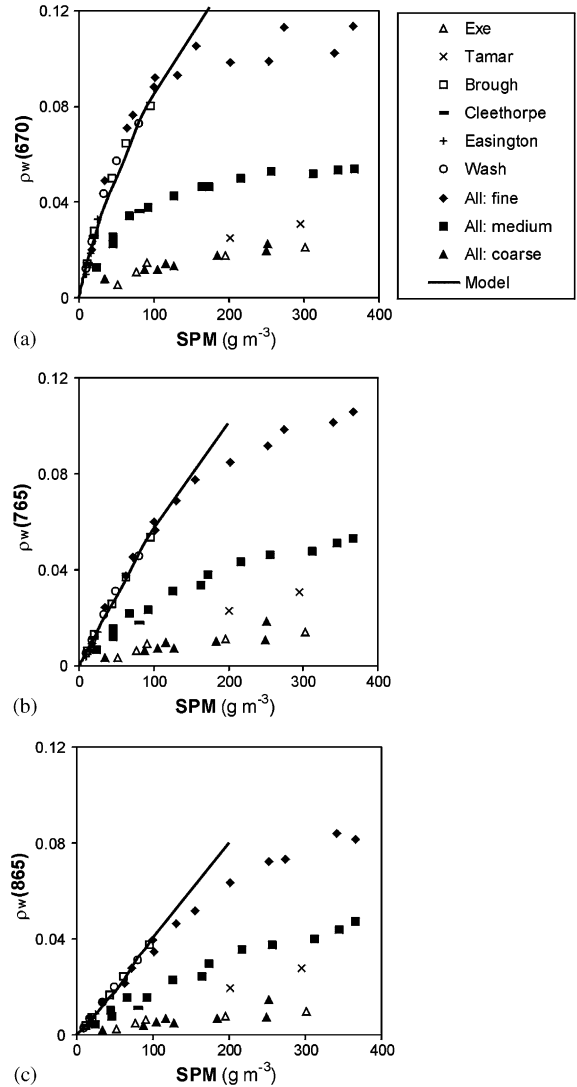


Fig. 1. Tank measurements of water reflectance at three SeaWiFS NIR wavebands for different SPM concentrations. (a) Reflectance at 670 nm. (b) Reflectance at 765 nm. (c) Reflectance at 865 nm. Results from a diverse range of sediment types from around the UK are shown: Exe estuary (Devon), Brough (Cumbria), Easington (Yorkshire), Tamar estuary (Devon), Cleethorpes (Lincolnshire) and the Wash (Lincolnshire). Data is shown for the entire sediment sample and for three size fractions: fine, medium and coarse. The coarse fraction settled 1 m in  $< 10$  min. The medium fraction settled 1 m in between 10 min and 3 h. The fine fraction took longer than 3 h to settle 1 m. The model developed to represent the SPM reflectance of the fine fraction up to  $200 \text{ g m}^{-3}$  is also shown—see text for more details.

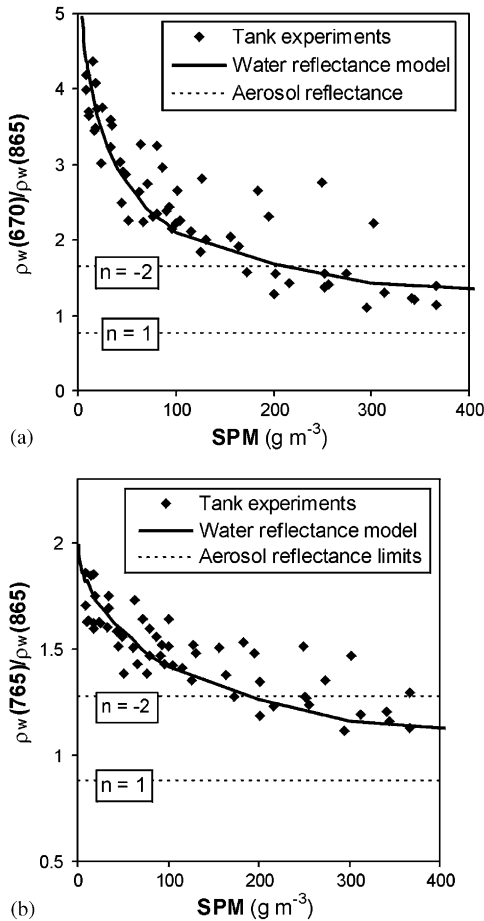


Fig. 2. Water reflectance and aerosol reflectance ratios in the NIR, shown as a function of the SPM parameter. (a) The ratio between the 670 and 865 nm bands. (b) The ratio between the 765 and 865 nm bands. The line shows the model developed to represent water reflectance when dominated by SPM. The aerosol reflectance ratios may lie anywhere region bounded by the dashed lines representing Ångström exponents ( $n$ ) of +1 to  $-2$ . The optical signature of the water and aerosol are indistinguishable where the water reflectance ratios lie between these lines.

largely determines water reflectance in the majority of SPM dominated natural waters. This decision is arbitrary. Actual total SPM concentration will tend to be greater than the model SPM parameter by an amount that depends on the particle size distribution of the particular sediment: the finer the sediment and the smaller the difference.

Absorption and backscatter by SPM in the model were taken as Eqs (6) and (7) respectively.

Note that the model is only applicable to the range  $0.1 < \text{SPM} < 200 \text{ g m}^{-3}$ .

$$a_{\text{SPM}}(\lambda) = a_{\text{SPM}}^*(\lambda) \text{SPM}^{0.32}, \quad (6)$$

$$b_{\text{SPM}}(\lambda) = 0.85 \text{SPM} \left( \frac{\lambda}{670} \right)^{-0.9}, \quad (7)$$

where the empirical constants are:  $a_{\text{SPM}}^*(\lambda) = [0.65, 0.45, 0.12]$  for  $\lambda = [670, 765, 865]$  respectively. A radiative transfer model, Hydrolight (Mobley, 1995), was used to obtain water reflectance from these absorption and scattering values for various sun positions and satellite viewing geometries. Pure water absorption data were taken from Pope and Fry (1997) and Palmer and Williams (1974), water scattering data were taken from Morel (1974), and the SPM scattering phase function of Petzold (1972) was used. The model results are shown in Figs. 1 and 2. The results were incorporated into a look-up table for use in the BP atmospheric correction method.

### 2.3. The Bright Pixel inversion model

The method used to partition the Rayleigh-corrected reflectance into aerosol and water reflectance is similar to that employed by the European MERIS satellite sensor (Moore et al., 1999), see Fig. 3 for an overview of the scheme. The MERIS method uses the NIR bands centred on 705, 775 and 865 nm, whereas the SeaWiFS method described here uses the 670, 765 and 865 nm bands. The significance of this band change is considered later.

Neglecting the effects of phytoplankton and CDOM on NIR reflectance, Eqs (3) and (5) give:

$$\begin{aligned} \rho_{\text{rc}}(\lambda) &= \rho_t(\lambda) - \rho_r(\lambda) \\ &= \rho'_a + t(\lambda)f(\lambda, \text{SPM}, \theta_0, \theta, \phi). \end{aligned} \quad (8)$$

Combining Eqs. (4) and (8) we can express the Rayleigh-corrected top-of-atmosphere reflectance ( $\rho_{\text{rc}}$ ) at 670 and 765 nm as two non-linear linked equations:

$$\begin{aligned} \rho_{\text{rc}}(670) &= \rho'_a(865) \left( \frac{670}{865} \right)^n \\ &+ t(670)f(670, \text{SPM}, \theta_0, \theta, \phi), \end{aligned} \quad (9)$$

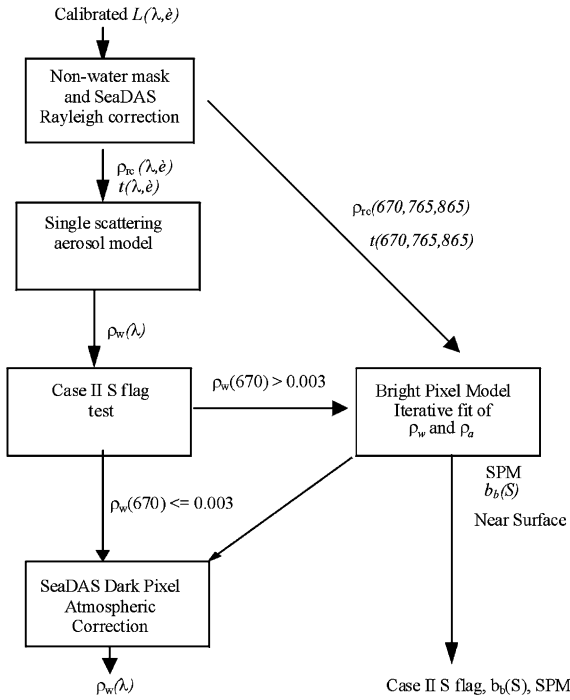


Fig. 3. Implementation of the BP atmospheric correction method for SeaWiFS within the SeaDAS version 4.1 processing scheme.

$$\rho_{rc}(765) = \rho'_a(865) \left( \frac{765}{865} \right)^n + t(765)f(765, SPM, \theta_0, \theta, \phi), \quad (10)$$

where we define:

$$\rho'_a(865) = \rho_a(865) + \rho_{ra}(865) = \rho_{rc}(865) - t(865)f(865, SPM, \theta_0, \theta, \phi). \quad (11)$$

Diffuse atmospheric transmittance is only a weak function of aerosol optical thickness and type, and the diffuse transmittance is assumed to be close to the original estimate of diffuse transmittance calculated by SeaDAS. Look-up tables generated from the modelling results Eqs. (9)–(11) to be solved by non-linear, least-squares, Newton–Raphson minimisation with backtracking in two-dimensional ( $n$  and SPM concentration) space (Press et al., 1992). The search method is started eight times from different initial guesses of  $n$ . The limits on the Ångström exponent and SPM

concentration are  $-1.5 < n < 0.5$  and  $0.1 < SPM < 200$ , respectively, which will cover the majority of natural conditions. The method generally required  $\sim 3$  iterations to converge per start. The best Ångström exponent and SPM values found by the search procedure are used to give water reflectance at 765 and 865 nm using the model look-up tables. The water reflectances are translated to the top of the atmosphere using the diffuse transmittance values calculated earlier. These  $t\rho_w$  values are subtracted from the  $\rho_{rc}$  values to give aerosol reflectances in the NIR. The SeaDAS DP atmospheric correction method (with phytoplankton-dependent NIR reflectance correction) is re-applied to extrapolate these NIR aerosol radiances to the visible bands.

The BP model requires more computing resource per pixel than the DP model because of the extra search procedure. This is generally not a problem because usually only a small proportion of pixels in an image are “Bright Pixels” and these can be pre-selected. First, non-water pixels (i.e. land and cloud) are excluded using the method of Lavender and Nagur (2002). The DP atmospheric correction model is then applied. A new flag, called the Case II Sediment (S) flag, is set for a pixel if the water reflectance at 670 nm, calculated on the DP basis and corrected to the top of the atmosphere, is greater than a threshold value. Moore et al. (1999) demonstrated that this approach, albeit using a band centred on 705 nm rather than 670 nm, was effective at identifying those pixels with an appreciable SPM concentration and non-zero NIR water reflectance. The revised threshold for 670 nm is set as 0.003.

There are two further implications of changes in the NIR bands between MERIS and SeaWiFS. First, unlike the MERIS 775 nm band, the SeaWiFS 765 nm band overlaps the oxygen A-band of absorption (Gregg et al., 1993, 1994; Barnes et al., 1994). Oxygen A-band absorption is corrected for in a two stage process following the SeaDAS approach (Ding and Gordon, 1995; Wang, 1999b). Second, phytoplankton absorption and scattering is strictly non-zero at 670 nm, implying that SPM is not solely responsible for water reflectance in the bands used for the BP

atmospheric correction. The significance of this is considered in detail below.

#### 2.4. In-situ data modelling

In-situ attenuation data was sampled during the passage of the Royal Research Ship (RRS) James Clark Ross (JCR) across an extensive coccolithophore bloom in the Western Approaches on the 15th June 2003. An approximate normalised water-leaving radiance,  $nL_w(\lambda)$ , was derived from measured attenuation as follows:

$$nL_w(\lambda) = F_0(\lambda) \frac{f}{Q} \left( \frac{b_b(\lambda) + c(\lambda)}{a_w(\lambda) + a_{ysbpa}(\lambda)} \right), \quad (12)$$

$$b_b(\lambda) = b_{bw}(\lambda) a, \quad (13)$$

$$c(\lambda) = \gamma(K(\lambda)), \quad (14)$$

$F_0(555)$  was assigned a value of  $185.33 \mu\text{W cm}^{-2} \text{nm}^{-1}$  and  $f/Q$  was approximated to 0.146 (estimated from Hydrolight). The absorption coefficients  $b_{bw}(\lambda)$  and  $a_w(\lambda)$  were taken from Pope and Fry (1997), and  $a_{ysbpa}(\lambda)$  from Kirk (1994). The constants  $\alpha$  and  $\gamma$  were assumed to be 0.5 and 0.017, respectively.

### 3. Results

#### 3.1. Performance of the iterative inversion method

A set of simulated  $\rho_{rc}$  data were generated to test the BP iterative inversion method. The simulated data had a uniformly distributed set of viewing geometries with a solar zenith angle between  $20\text{--}50^\circ$ , a sensor zenith angle between  $30\text{--}50^\circ$  and azimuth differences between solar and sensor position of  $0\text{--}180^\circ$ . SPM concentration was allowed to vary randomly between 0.1 and  $200 \text{ gm}^{-3}$ , with a log-uniform distribution to approximate natural variation.  $\rho'_a(865)$  was allowed to vary uniformly between 0.005 and 0.030. Rayleigh-corrected reflectances at SeaWiFS bands 6–8 were modelled assuming that all water reflectance is due to water and sediment, no absorption except by water, and aerosol radiances that follow Eq. (4). Varying amounts of noise

(between 0 and 5%) were introduced to the modelled  $\rho_{rc}$  values for NIR bands to simulate absolute SeaWiFS measurement uncertainties.

The calibration of the SeaWiFS sensor is monitored by the SeaWiFS project team in a number of ways, including in-orbit methods (lunar and solar viewing; Barnes et al., 2001), and using vicarious calibration facilities such as the Marine Optical Buoy (Clark et al., 1997). Wang and Gordon (2002) showed that given such methods it should be possible to obtain the water-leaving reflectances at the blue to 5%. This is confirmed by SeaWiFS post-launch validation analyses (e.g. McClain et al., 2000; Barnes et al., 2001; Eplee et al., 2001) which show non-systematic (and hence uncorrected) variations in the gain of the NIR bands to be  $<1.5\%$ , suggesting that uncertainties in the absolute values of  $\rho_{rc}(\text{NIR})$  are less than  $\sim 3\%$ .

Modelled Rayleigh-corrected reflectances with these superimposed uncertainties were passed to the BP model for inversion, and the results are shown in Fig. 4. The retrieval of the Ångström exponent and aerosol reflectance follow the same pattern as the retrieval of SPM. The performance of the inversion method in retrieving water reflectance at 765 and 865 nm from modelled, noisy, Rayleigh-corrected top-of-atmosphere reflectance is summarised in Table 1.

The retrieval performance is excellent when there is no measurement noise: the mean difference is  $<0.2\%$ , the root-mean-square (RMS) difference is  $\sim 10\%$  and over 95% of the retrievals are within 20% of the actual value. The few failures in the inversion method arise because more than one combination of SPM, Ångström exponent and aerosol reflectance give the same Rayleigh-corrected reflectances at 670, 765 and 865 nm. The presence of a non-unique solution to the inversion problem becomes more problematic at SPM concentrations greater than c.  $50 \text{ gm}^{-3}$  and the performance of the inversion method is consequently worse at these high SPM values. The efficacy of the retrieval decreases significantly with only small amounts of measurement noise because more there are more alternative good solutions. At 0.5% of noise, the RMS difference has increased to  $\sim 30\%$  and less than 70% of the retrievals are

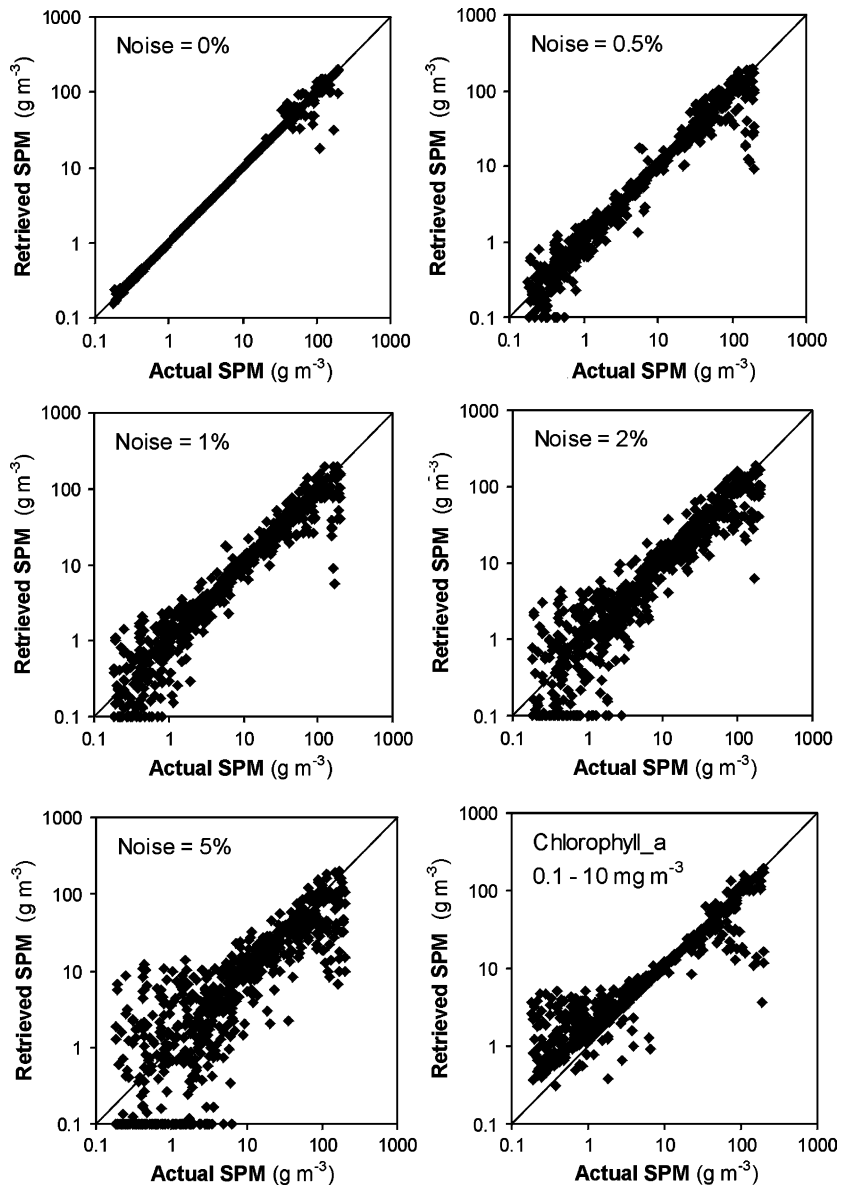


Fig. 4. The performance of the BP atmospheric correction method in inverting modelled Rayleigh-corrected NIR reflectances to SPM concentration. The various graphs represent the effect of increasing the amounts of measurement noise from 0% to 5%. The performance of the method in obtaining the SPM concentration gradually deteriorates as the noise increases. The effect of co-occurring phytoplankton (equivalent in concentration to between 0.1 and 10  $\text{mg m}^{-3}$  of chlorophyll-*a*) is shown in the last panel. The inversion method is very sensitive to noise in the measurement of top-of-atmosphere reflectance for reasons discussed in the text, but less sensitive to phytoplankton.

within 20%. At 5% of measurement noise, the RMS error in the retrieval is more than 25% and <30% of the retrievals are within 20% of the

actual values. This reduction in inversion performance in response to measurement error is a fundamental limitation of the pixel-by-pixel,

Table 1

The performance of the Bright Pixel inversion method in retrieving water reflectance at 765 and 865 nm from modelled Rayleigh-corrected top-of-atmosphere reflectance as described in the text

Noise (%)	$\rho_w(765)$			$\rho_w(865)$		
	Mean difference (%)	RMS difference (%)	Fraction within 20%	Mean difference (%)	RMS difference (%)	Fraction within 20%
0	-0.1	9.2	0.95	-0.2	10.6	0.95
0.5	-0.8	31.2	0.55	-1.1	33.7	0.68
1	-4.8	50.7	0.56	-5.5	54.8	0.52
2	-14.5	98.7	0.42	-16.6	108.4	0.40
5	-44.8	263.8	0.29	-52.3	301.2	0.27
Chl-a <sup>a</sup>	-70.0	195.3	0.50	-77.3	220.2	0.48

The effect of difference amounts of measurement noise on the retrieval is shown.

<sup>a</sup>Phytoplankton co-occurring with SPM. Chlorophyll-*a* concentration between 0.1 and 10 mg m<sup>-3</sup>.

search-based approach using only the NIR bands, and is not a function of the particular search method employed.

SeaWiFS aims for <1% relative uncertainty (i.e. between bands) in the measurement of top-of-atmosphere reflectance and recent validation work suggests that the mission is achieving this aim (Barnes et al., 2001; Eplee et al., 2001). Our work suggests that this would imply an RMS error in the estimated NIR water reflectance in SPM dominated waters of ~40%.

### 3.2. Model sensitivity to co-occurring phytoplankton

The BP atmospheric correction method described here assumes that all water reflectance between 670 and 865 is due to suspended inorganic matter and water itself. Phytoplankton can grow in turbid waters and may absorb in this spectral region. The effect of phytoplankton co-occurring with inorganic sediment on NIR reflectance was investigated experimentally by adding different concentrations of phytoplankton cultures to sediment in a series of tank experiments as described previously (Fig. 5). The lines representing different phytoplankton concentrations converge above ~700 nm suggesting that phytoplankton pigments absorb light up to about 700 nm but do not significantly affect reflectance at longer wavelengths. The model sensitivity to co-occurring

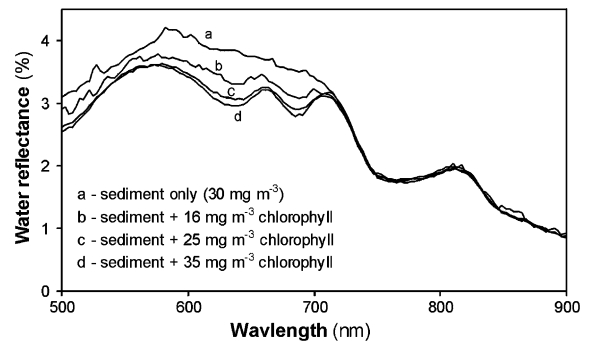


Fig. 5. Water reflectance spectra measured by a spectroradiometer during a series of tank experiments as described in the text. Varying concentrations of phytoplankton were added to inorganic sediment in the water, which is stirred before measurement. The effect of phytoplankton on the water reflectance is restricted to wavelengths shorter than ~700 nm.

phytoplankton was investigated theoretically by estimating the absorption and scattering in the NIR by phytoplankton cells and including these with the SPM inherent optical properties. At chlorophyll-*a* concentrations of 0.1, 1, 10 and 40 mg m<sup>-3</sup>, absorption at 770 nm was taken as 0.002, 0.020, 0.19 and 0.75 m<sup>-1</sup>, scatter at 770 nm as 0.060, 0.25, 1.03, 2.43 m<sup>-1</sup>, and scatter is taken as being proportional to  $\lambda^{-1}$ , consistent with published field measurements (e.g. Moore et al., 1999). The changes in the ratio of NIR reflectances are shown in Fig. 6 and confirm that the 765:865

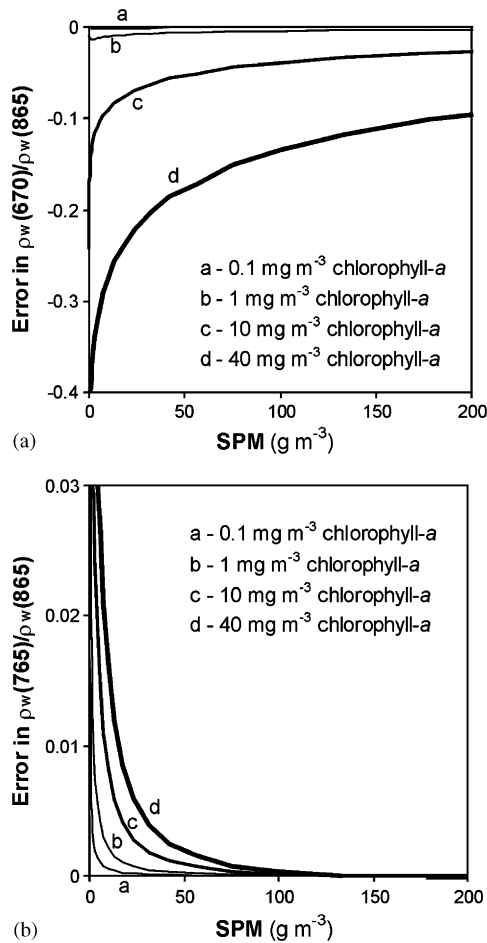


Fig. 6. The sensitivity of the modelled NIR water reflectances to phytoplankton coexisting with SPM. (a) The effect of different concentrations of phytoplankton on the  $\rho_w(670)/\rho_w(865)$  ratio. (b) The effect of phytoplankton on the  $\rho_w(765)/\rho_w(865)$  ratio. The graphs show the change in the NIR reflectance ratios as a proportion of the value if there were no phytoplankton present.

water reflectance ratio is insensitive to the presence of phytoplankton. The small positive bias (<3%) is due to the extra scattering by phytoplankton cells and detritus. The 670:865 water reflectance ratio is more sensitive to the presence of phytoplankton. Phytoplankton have a significant effect (>10%) on the 670:865 water reflectance ratio at low SPM concentrations (<7 g m<sup>-3</sup>) or at high Ca concentrations (>35 mg m<sup>-3</sup>). Where moderate or low Ca concentrations (<35 mg m<sup>-3</sup>) co-occur

with moderate or high SPM concentrations (>7 g m<sup>-3</sup>), the negative bias due to phytoplankton on the 670:865 water reflectance ratio is less than 10%. The effect of phytoplankton on SPM retrieval by the BP method was tested by generating simulated Rayleigh-corrected NIR top-of-atmosphere reflectance due to sediment and co-occurring phytoplankton (equivalent to a chlorophyll-*a* concentration of between 0.1 and 10 mg m<sup>-3</sup>). The results of the retrieval are shown in the last panel of Fig. 5, and the last row of Table 1. Phytoplankton caused the BP atmospheric correction method to overestimate SPM at low SPM concentrations, but had little effect at SPM concentrations >10 g m<sup>-3</sup>. The BP modification is vanishingly small as SPM approaches 0.1 g m<sup>-3</sup> and inaccuracies in the estimation of SPM at these low concentrations due to co-occurring phytoplankton are acceptable.

### 3.3. Validation of the Bright Pixel model

The BP model can be validated qualitatively by comparing water-leaving radiance spectra in Case 2 regions with spectra produced using the DP atmospheric correction algorithm. SeaWiFS images with low proportions of cloud cover were selected from the period May–August 2001 (sequential day of year 127–240), in four European regions that are often Case 2: Thames Estuary, the outflow of the Gironde Estuary (Doxaran et al., 2002) into the Bay of Biscay, German Bight and Netherlands coast (Eisma and Kalf, 1979), Bristol Channel and the Western approaches of the Approaches (Table 2). SeaWiFS full resolution (1.1 km) HRPT data were used, and these were received by the Dundee Satellite Receiving Station and processed at the University of Plymouth. The original (DP) and modified (BP) versions of SeaDAS 4.1 were used to generate SeaWiFS Level 2 files containing  $nL_w$  at all wavelengths, chlorophyll-*a* concentration, and diffuse attenuation at 490 nm from each SeaWiFS Level 1 file (top of atmosphere reflectance data). The total number of pixels which required the BP atmospheric correction in these five images was 11212. There was no difference in any of these products for pixels that did not activate the BP flag, as expected.

Table 2  
Regions used to validate the Bright Pixel atmospheric correction code in European waters

Region	Date	SeaWiFS L1 file	N limit	S limit	W limit	E limit	Number of BP
Thames Estuary	8 May 2001	S2001128120907	52.5	51.0	0.5	3.0	3236
Gironde outflow	19 June 2001	S2001170123127	47.5	45.0	−3.0	−0.8	1270
German Bight and Netherlands coast	5 July 2001	S2001186122533	53.8	51.2	3.0	6.0	2325
Bristol Channel	27 August 2001	S2001239135956	51.8	51.0	−5.0	−2.5	891
Western Approaches	15 June 2003	S2003166124428	51.6	48.5	−7.4	−2.5	3992

The SeaWiFS Level 1 HRPT file from the Dundee satellite receiving station is shown, and the number of pixels which required the Bright Pixel modification for atmospheric correction.

Fig. 7 shows the result of applying the BP atmospheric correction model to the five test images given in Table 2. Columns 1 and 2 show the effect of changing from the DP to the BP atmospheric correction model on the  $nL_w(412)$  product. This product has been chosen because the effect of ignoring water reflectance in the NIR is greatest at the shorter wavelengths of the visible spectrum. Fig. 7 column 3 shows the predicted SPM concentrations for the pixels that were atmospherically corrected by the BP modified method.

The BP modifications increased the  $nL_w$  (i.e. water reflectance) value across the whole spectrum (Fig. 8). The average differences were larger in the blue (mean increase of  $1.3 \mu\text{W cm}^{-2} \text{sr}^{-1} \text{nm}^{-1}$  at 412 nm) and smaller towards the red (mean increase of  $0.7 \mu\text{W cm}^{-2} \text{sr}^{-1} \text{nm}^{-1}$  at 555 nm). Similar  $nL_w$  increases were found over the coccolithophore bloom due to atmospheric correction modification. The averaged percentage difference between the original DP and the BP atmospheric correction can reach 14% in the blue part of the spectrum and more than 50% in the NIR. Also, comparisons between BP and derived  $nL_w$  from in-situ attenuation data across the whole transect (Fig. 9) have led to an averaged difference of less than 30% and 50% at 555 and 670 nm respectively, whereas the DP estimates for the same wavelengths were slightly higher (35% and 69% for the same wavelengths).

The negative  $nL_w$  values in the blue part of the spectrum produced by the SeaDAS 4.1 DP atmospheric correction code are erroneous and result in

part from not taking into account that water leaving radiance in the NIR is non-zero in some cases. The BP model elevated  $nL_w$  values and led to fewer spectra having negative water leaving radiances in the blue part of the spectrum than the original DP atmospheric correction scheme. This is a significant improvement in the atmospheric correction of ocean colour images of turbid waters.

The pixel-by-pixel effect of the BP modification with respect to the DP method for the  $nL_w(412)$  product is shown in Fig. 10. The pixels above the dashed 1:1 line are those where the BP modification has worked effectively. The values very close to, or even below, the 1:1 line are those where the method has estimated an SPM concentration which is much lower than the true value. In these cases, the correction for non-zero NIR water reflectance is much too small and only serves to skew the  $\rho_{rc}(765)$  and  $\rho_{rc}(865)$  values leading to poor estimates of  $\rho_w$  in the visible spectrum. The failures account for less than 12% of the total pixels processed by the BP method. The success rates were 81%, 98%, 94% and 82% for the Thames estuary, Gironde outflow, German Bight/Netherlands coast, and Bristol Channel regions respectively. The failure rate suggests that the effective noise level in SeaWiFS measurements of NIR reflectance is  $\sim 0.15\%$ .

SeaWiFS measurements of both chlorophyll-*a* concentration (from the standard SeaWiFS OC4v4 algorithm) and diffuse attenuation (from the SeaWiFS operational algorithm) tended to decrease when the BP modification was applied, by

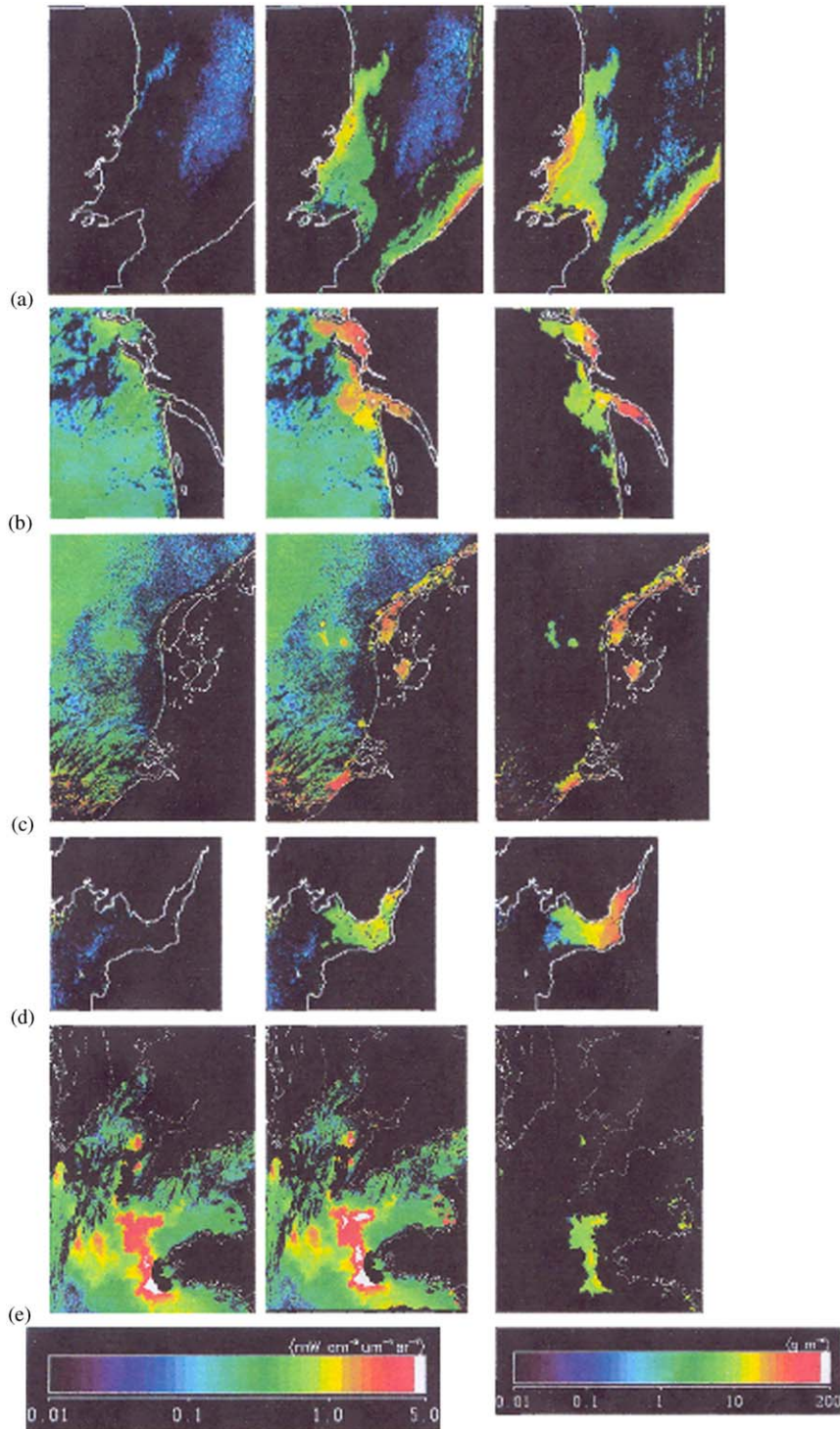


Fig. 7. Comparison of the SeaWiFS  $nL_w(412)$  product for five European regions, showing the effect of the DP (1st column) and BP (2nd column) atmospheric correction methods and the resulting SPM concentration (3rd column). (a) Thames estuary. (b) Gironde estuary outflow. (c) German Bight and Netherlands coast. (d) Bristol Channel. (e) Western Approaches. All  $nL_w(412)$  images share the same normalised radiance scale and all SPM images share the same SPM scale.

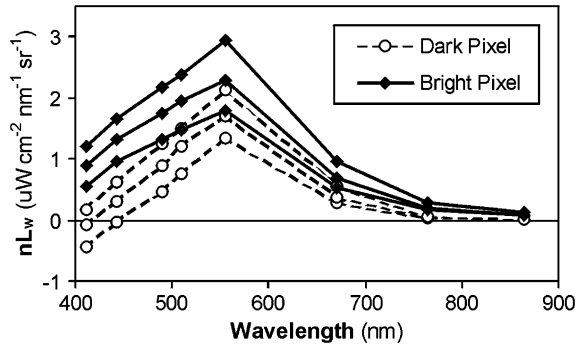


Fig. 8. The effect of the BP atmospheric correction modification on the normalised water leaving spectra for those pixels flagged as having significant inorganic SPM in four European regions. The figure shows (from top) the upper-quartile, mean and lower quartile  $nL_w$  spectra for 7700 pixels. The broken lines and open symbols show spectra produced using the original, DP SeaWiFS atmospheric correction method. The solid lines and filled symbols show the result of using the BP method. The increase of  $nL_w$ , especially at the blue end of the spectrum, represents a considerable improvement.

55% and 48%, respectively. In Case 2 waters,  $nL_w$  in the blue spectral region will be underestimated by more than  $nL_w$  in the green region, leading to overestimates of both products. It must be noted that both algorithms are applicable only to Case 1 waters, and the BP corrected values, although better than those relying on the DP method, will still be erroneous.

#### 4. Discussion and conclusions

The laboratory experiments (Fig. 2) highlighted the well-behaved relationship between the NIR reflectance ratios and SPM, and that it was possible to distinguish the SPM reflectance from the aerosol reflectance at SPM concentrations of less than  $200 \text{ g m}^{-3}$ . The BP inversion method can be used to partition the Rayleigh-corrected reflectance between aerosol and water reflectance, so that the water reflectance can be removed and the pixel passed through the SeaDAS DP atmospheric correction. The major differences between the SeaWiFS and MERIS (Moore et al., 1999) implementations were that SeaWiFS has no band at around 700 nm so the 670 nm band is used

instead, and the SeaWiFS 765 nm waveband overlaps the oxygen A-band of absorption so this must be accounted for.

The simulated data demonstrated that the BP iterative inversion method worked effectively when there was no noise, but that the performance decreased significantly as measurement noise was added. However, the approach works well within the capabilities of SeaWiFS i.e. well at an absolute noise level of 1% and acceptably at a level of 2%. The model was also shown to be relatively insensitive to the co-occurrence of phytoplankton, which might have been a problem because of the use of a visible waveband (670 nm).

Difficulties of making NIR measurements in the field (Section 2.2) have led to scarce in-situ data for validation of the BP approach. The five chosen sites (Thames Estuary, Gironde Estuary, German Bight/Netherlands coast, Bristol Channel and Western Approaches) demonstrated an increase in the remotely sensed normalised water-leaving radiance when the BP approach was used and significantly fewer pixels had negative values in the blue part of the spectrum. Although coincident in-situ measurements, for the Western Approaches, from latitude  $49^{\circ}5$  to  $49^{\circ}7\text{N}$  do not seem to lead to a better fit between modelled in-situ  $nL_w$  values and satellite estimates, the response of the BP model to particulate calcite due to a coccolithophore bloom event has shown to agree relatively well with the derived  $nL_w$  values, suggesting a better performance of the BP model over high scattering waters compared to the DP.

Further research will be carried out to assess the BP approached quantitatively with respect to field measurements. The BP modified atmospheric correction method is being applied to compact airborne spectrographic imager (CASI) imagery so that a multi-height approach can be applied to the validation (Lavender and Nagur, 2002). Additional laboratory measurements, together with in-situ measurements, will be taken to further develop the SPM modelling. Given the sensitivity of the model to SeaWiFS noise it is also important that the SeaWiFS measurement uncertainties are quantified by ongoing vicarious radiometric validation studies.

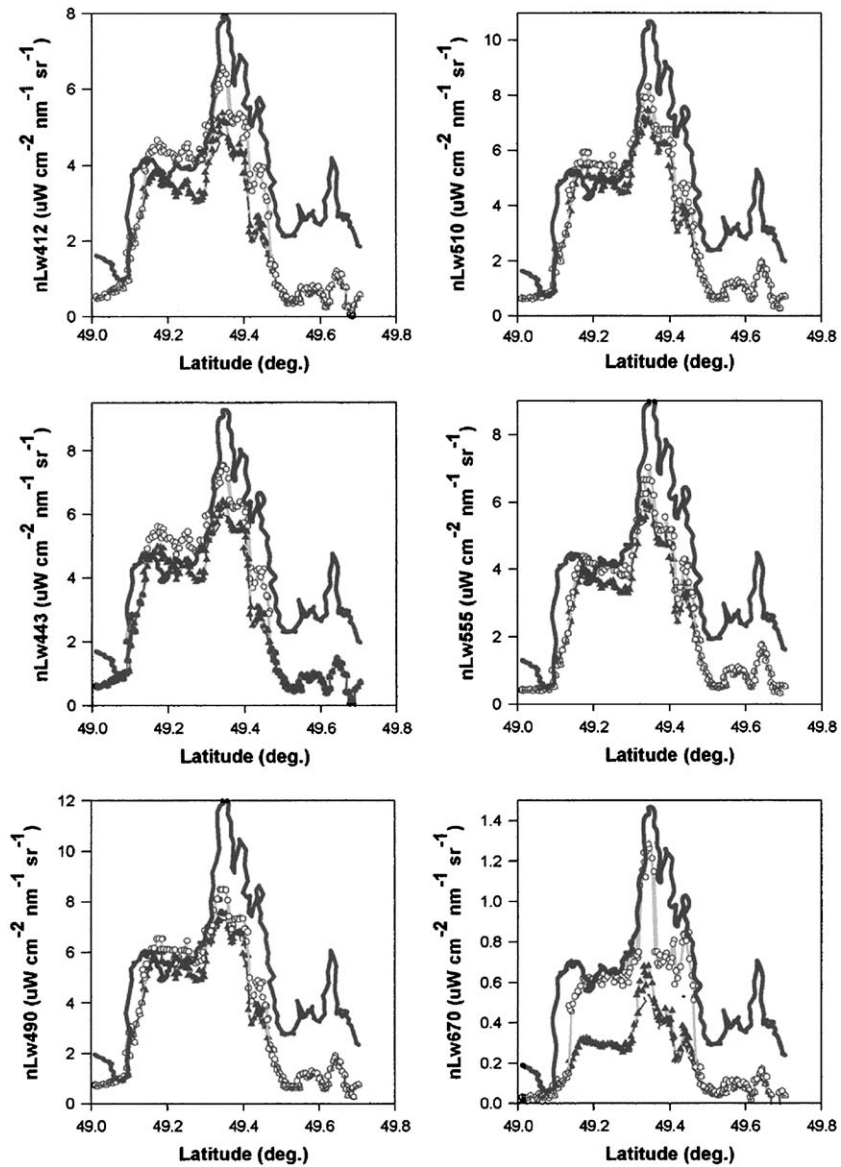


Fig. 9. Normalised water-leaving radiance ( $nL_w$ ) response comparison over a coccolithophore bloom for 6 SeaWiFS wavebands: derived-in situ  $nL_w$  (—), with DP atmospheric correction (—▲—) and with BP atmospheric correction (—○—).

## Acknowledgements

This work was part-funded through the Natural Environment Research Council SeaWiFS Exploitation Initiative and has also been supported

through NERC Centre for Observation of Air-Sea Interactions and Fluxes (CASIX contribution number 31). The authors would like to thank Alex Cunningham (University of Strathclyde) for useful discussions. The SeaWiFS satellite mission is a

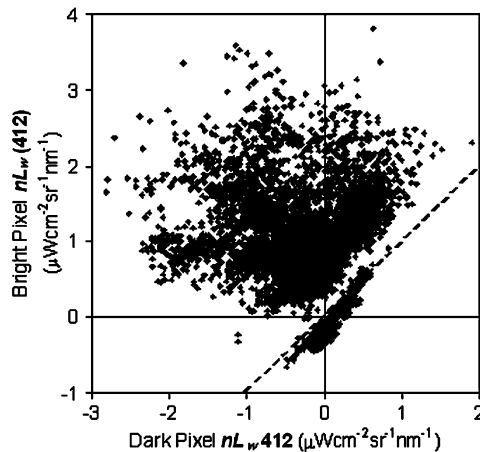


Fig. 10. The effect of the BP modification on the SeaWiFS  $nL_w(412)$  product for those 7700 pixels flagged as having non-zero water reflectance in the NIR in four of the five European regions (excludes Western English Channel). The figure shows  $nL_w(412)$  produced by the BP atmospheric correction method as a function of the original value. The 1:1 line is shown dashed. Values above the 1:1 line represent successful performance of the BP method, and account for 88% of the total points shown. The values very close to or below the 1:1 line are those which have appreciable concentrations of SPM but for which the BP method has failed. See text for discussion.

joint venture of Orbital Sciences Corporation and NASA. Information on the method used by SeaWiFS to correct for the effects of oxygen absorption was used courtesy of the Rosenstiel School of Marine and Atmospheric Science, University of Miami, Florida. Tank reflectance spectra were measured with equipment loaned from the NERC Equipment Pool for Field Spectroscopy.

## References

- Aiken, J., Rees, N., Hooker, S.B., Holligan, P., Bale, A.J., Robins, D.B., Moore, G., Harris, R.P., Pilgrim, D.A., 2000. The Atlantic Meridional Transect: overview and synthesis of data. *Progress in Oceanography* 45, 257–312.
- Bale, A.J., Tocher, M.D., Weaver, R., Hudson, S.J., Aiken, J., 1994. Laboratory measurements of the spectral properties of estuarine suspended particles. *Netherlands Journal of Aquatic Ecology* 28, 237–244.
- Barnes, R.A., Holmes, A.W., Barnes, W.L., Esaias, W.E., McClain, C.R., Svitek, T., 1994. SeaWiFS pre-launch radiometric calibration and spectral characterisation. In: Hooker, S.B., Firestone, E.R. (Eds.), *NASA Technical Memo 104566*, vol. 23. NASA Goddard Space Flight Centre, Greenbelt, MA, p. 55.
- Barnes, R.A., Eplee, R.E., Schmidt, M., Patt, F.S., McClain, C.R., 2001. Calibration of SeaWiFS. 1. Direct techniques. *Applied Optics* 40, 6682–6700.
- Clark, D.K., Gordon, H.R., Voss, K.J., Ge, Y., Broenkow, W., Trees, C.C., 1997. Validation of atmospheric correction over the oceans. *Journal of Geophysical Research* 102, 17209–17217.
- Ding, K., Gordon, H.R., 1995. Analysis of the influence of  $O_2$  A-band absorption on atmospheric correction of ocean color imagery. *Applied Optics* 34, 2068–2080.
- Doxaran, D., Froidefond, J.M., Lavender, S.J., Castaing, P., 2002. Spectral signature of highly turbid waters. Application with SPOT data to quantify suspended particulate matter concentrations. *Remote Sensing of Environment* 81, 149–161.
- Eisma, D., Kalf, J., 1979. Distribution of particle size of suspended matter in the southern bight of the North Sea and the eastern channel. *Netherlands Journal of Sea Research* 13 (2), 289–324.
- Eplee, R.E., Robinson, W.D., Bailey, S.W., Clark, D.K., Werdell, P.J., Wang, M., Barnes, R.A., McClain, C.R., 2001. Calibration of SeaWiFS. 2. Vicarious techniques. *Applied Optics* 40, 6701–6718.
- Fu, G., Baith, K.S., McClain, C.R., 1998. SeaDAS: The SeaWiFS Data Analysis System, *Proceedings of The 4th Pacific Ocean Remote Sensing Conference*, Qingdao, China, 28–31 July 1998, pp. 73–79.
- Gordon, H.R., Wang, M., 1992. Surface roughness considerations for atmospheric correction of ocean colour sensors. 1: the Rayleigh scattering component. *Applied Optics* 31, 4247–4260.
- Gordon, H.R., Wang, M., 1994a. Retrieval of water-leaving radiance and aerosol optical thickness over oceans with SeaWiFS: a preliminary algorithm. *Applied Optics* 33, 443–452.
- Gordon, H.R., Wang, M., 1994b. Influence of oceanic whitecaps on atmospheric correction of ocean-colour sensor. *Applied Optics* 33, 7754–7763.
- Gordon, H.R., 1997. Atmospheric correction of ocean colour imagery in the Earth Observing system era. *Journal of Geophysical Research* 102, 17081–17106.
- Gordon, H.R., Brown, O.B., Evans, R.H., 1988. Exact Rayleigh scattering calculations for use with the Nimbus-7 Coastal Zone Color Scanner. *Applied Optics* 27, 862–871.
- Gordon, H.R., Brown, O.B., Evans, R.H., Brown, J.W., Smith, R.C., Baker, K.S., Clark, D.K., 1988. A semianalytic radiance model of ocean colour. *Journal of Geophysical Research* 93 (D9), 10909–10924.
- Gordon, H.R., Clark, D.K., Brown, J.W., Brown, O.B., Evans, R.H., Broenkow, W.W., 1983. Phytoplankton pigment concentrations in the Middle Atlantic Bight: Comparison between ship determinations and coastal zone color scanner estimates. *Applied Optics* 22, 20–36.

- Gordon, H.R., Ding, K., 1992. Self-shading of in-water optical instruments. *Limnology and Oceanography* 37, 491–500.
- Gregg, W.W., Chen, F.C., Mezaache, A.L., Chen, J.D., Whiting, J.A., 1993. In: Hooker, S.B., Firestone, E.R. (Eds.), NASA Technical Memo 194566, vol. 9. NASA Goddard Space flight Centre, Greenbelt, MA, p. 17.
- Gregg, W.W., Patt, F.S., Woodward, R.H., 1994. The simulated SeaWiFS data set. Version 2. In: Hooker, S.B., Firestone, E.R. (Eds.), NASA Technical Memo 194566, vol. 15. NASA Goddard Space flight Centre, Greenbelt, MA, p. 24.
- Hooker, S.B., Esaias, W.E., Feldman, G.C., Gregg, W.W., McClain, C.R., 1992. An overview of SeaWiFS and ocean colour. In: Hooker, S.B., Firestone, E.R. (Eds.), NASA Technical Memo 104566, vol. 1. NASA Goddard Space Flight Centre, Greenbelt, MA, p. 24.
- Hooker, S.B., Lazin, G., Zibordi, G., McClean, S., 2002. An evaluation of above- and I-water methods for determining water-leaving radiances. *Journal of Atmospheric and Oceanic Technology* 19, 486–515.
- Kirk, J.T.O., 1994. *Light and Photosynthesis in Aquatic Ecosystems*. Cambridge University Press, Cambridge 509pp.
- Lavender, S.J., Nagur, C.R.C., 2002. Mapping Coastal Waters with High Resolution Imagery: atmospheric correction of multi-height airborne imagery. *Journal of Optics A: Pure and Applied Optics* 4, S50–S55.
- McClain, C.R., Ainsworth, E.J., Barnes, R.A., Eplee, R.E., Patt, F.S., Robinson, W.D., Wang, M., Bailey, S.W., 2000. SeaWiFS postlaunch calibration and validation analyses, part 1, SeaWiFS Postlaunch Technical Report Series, Vol. 9, Greenbelt, MA, NASA Goddard Space Flight Center, Greenbelt, USA, 82pp.
- Mobley, C.D., 1995. *Hydrolight 3.0 Users Guide*, SRI Project 5632.
- Moore, G.F., Aiken, J., Lavender, S.J., 1999. The Atmospheric correction of water colour and the quantitative retrieval of suspended particulate matter in case 2 waters: application to MERIS. MERIS Special Issue. *International Journal of Remote Sensing* 20, 1713–1733.
- Morel, A., 1974. Optical properties of pure water and pure sea water. In: Jerlov, N.G., Nielsen, E.S. (Eds.), *Optical Aspects of Oceanography*. Academic, San Diego, USA, pp. 1–24.
- Palmer, K.F., Williams, D., 1974. Optical properties of the water in the near infra-red. *Journal of the Optical Society of America* 64, 1107–1110.
- Petzold, T.J., 1972. Volume scattering functions for selected ocean waters. *Scripps Institute of Oceanography Report* 79, 72–78.
- Pope, R.M., Fry, E.S., 1997. Absorption spectrum (380–700 nm) of pure water. II. Integrating cavity measurements. *Applied Optics* 36, 8710–8723.
- Press, W.H., Teukolsky, S.A., Vetterling, W.T., Flannery, B.P., 1992. *Newton-Raphson method for non-linear systems of equations*. *Numerical Recipes in C*, second ed. Cambridge University Press, Cambridge 379–393.
- Ruddick, K.G., Ovidio, F., Rijkeboer, M., 2000. Atmospheric correction of SeaWiFS imagery for turbid and inland waters. *Applied Optics* 39, 897–912.
- Siegel, D.A., Wang, M., Maritorena, S., Robinson, W., 2000. Atmospheric correction of satellite ocean color imagery: the black pixel assumption. *Applied Optics* 39, 3582–3591.
- Wang, M., 1999a. Atmospheric correction of ocean colour sensors: computing atmospheric diffuse transmittance. *Applied Optics* 38, 451–455.
- Wang, M., 1999b. Validation study of the SeaWiFS oxygen A-band absorption correction: comparing the retrieved cloud optical thicknesses from SeaWiFS measurements. *Applied Optics* 38, 937–944.
- Wang, M., 2000. The SeaWiFS atmospheric correction algorithm updates, SeaWiFS postlaunch calibration and validation analyses, Part 1, vol. 9, NASA Goddard Space Flight Centre, Greenbelt, USA, pp. 57–63.
- Wang, M.H., Gordon, H.R., 2002. Calibration of ocean color scanners: how much error is acceptable in the near infrared? *Remote Sensing of Environment* 82 (2–3), 497–504.